Penning Ionization of CH_3SCH_3, CH_3SSCH_3, and CH_3CH_2SH by Collision with He*(2^3S) Metastable Atoms

Naoki Kishimoto, Ryoji Yokoi, Hideo Yamakado, and Koichi Ohno*

Department of Chemistry, Graduate School of Science, Tohoku University, Aoba-ku, Sendai 980-77, Japan

Received: January 9, 1997; In Final Form: February 28, 1997[⊗]

Penning ionization of CH_3SCH_3 (dimethyl thioether), CH_3SSCH_3 (dimethyl disulfide), and CH_3CH_2SH (ethyl thioalcohol) upon collision with He*(2^3S) metastable atoms was studied by two-dimensional (electron-energy/collision-energy-resolved) Penning ionization electron spectroscopy. A collision energy dependence of the partial ionization cross sections has indicated that the interaction potentials are anisotropic between He*(2^3S) and the target molecules. For CH_3SCH_3 and CH_3CH_2SH, the interaction potential around the sulfur atom was found to be more attractive for the out-of-plane direction vertical to the CSC or CCS plane than for the in-plane direction, while the opposite trend was observed around the oxygen atom of CH_3CH_2OH. Anisotropic potential for CH_3SSCH_3 was found to be similar to that for CH_3SCH_3. Strongly enhanced bands in Penning ionization electron spectra of sulfur compounds, which were assigned to ionization from molecular orbitals having sulfur 3s (S_{3s}) atomic orbital character, were found to be associated with an intermolecular excitation transfer from He* to the target molecule and also with the following intramolecular Auger-like autoionization process.

I. Introduction

When a metastable atom A* collides with a target molecule M, where A* has an excitation energy larger than the lowest ionization potential (IP) of M, a chemi-ionization process known as Penning ionization[1] can occur:

$$M + A^* \rightarrow M^+ + A + e^- \quad (1)$$

In the electron exchange model of Penning ionization process proposed by Hotop and Niehaus,[2] an electron in a molecular orbital (MO) which has large electron densities outside the surface of M is transferred to the inner-shell orbital of colliding A*, and the excited electron in A* is ejected. Branching ratios in Penning ionization for various ionic states are reflected in the band intensities of kinetic energy distribution of ejected electrons observed by Penning ionization electron spectroscopy.[3−5] It has been shown from the study of Penning ionization electron spectroscopy of polyatomic molecules that the most effective approaching directions for the collisional ionization are different depending upon the electron distribution of the target MOs and that band intensities in Penning ionization electron spectra (PIES) are approximately proportional to the probed electron densities.[6] Some exceptional cases besides the exchange type Penning ionization process,[2] however, have been found to have a relation to $\pi-\pi^*$ excitation,[7−10] an avoided surface crossing to ion-pair potential,[11] or an Auger-like autoionization transition involving electronic transition from an upper occupied MO to an inner hole in the target molecule.[12]

Previously, Ohno et al. have performed simple quantitative calculations on branching ratios in the exchange type Penning ionization by an exterior electron density (EED) model[6,12,13] using *ab initio* molecular orbital functions. In the EED model, exterior electron densities (EED) are defined for individual MOs

$$(\mathrm{EED})_i = \int_\Omega |\phi_i(r)|^2 \, dr \quad (2)$$

where Ω is the subspace outside the repulsive molecular surface and ϕ_i is the respective MO to be ionized. Calculated EED values have been found to be in good agreement with the observed band intensities of PIES for some molecules on the assumption of the repulsive molecular surface as rigid van der Waals spheres. Basis set dependence of the calculated EED values was also investigated.[14] The deflection of trajectories of metastable atoms by attractive force or the anisotropic change of the repulsive surface of a target molecule, however, must be considered in order to estimate branching ratios (partial ionization cross sections) for the exchange type Penning ionization that depend on collision energies.

In this connection, a collision energy dependence of the partial ionization cross sections (CEDPICS) has been observed by collision-energy-resolved Penning ionization electron spectroscopy[7−12,15−23] which was introduced for atomic targets by Hotop et al.[24] Different from a collision energy dependence of the total ionization cross sections observed by detection of ion signals,[25−32] the state-resolved measurement of CEDPICS enables us to investigate the anisotropic potential energy surface around the target molecule since the electron distribution of the individual MOs is more or less localized on a special part of the molecule. Attractive interactions with He* were found for local regions around the oxygen atom of CH_3OH, CH_3OCH_3, and $(CH_3CH_2)_2O$.[20] For CH_3OCH_3, the interaction potential energy was calculated to be more attractive for the in-plane direction than for the out-of-plane direction vertical to the COC plane.[20] In addition, strong negative collision energy dependence was observed for H_2O and H_2S.[11] Strong attractive interactions, however, were not found around the sulfur atom of CH_3NCS[18] and thiophene.[10] Systematic investigations are thus required for anisotropic interactions between He* and sulfur compounds.

In this study, we investigated interactions between He* and aliphatic sulfur compounds (CH_3SCH_3, CH_3SSCH_3, CH_3CH_2SH) by two-dimensional (electron-energy/collision-energy-resolved) Penning ionization electron spectroscopy.[21] For a comparative study, anisotropic interaction potentials around the oxygen atom of ethanol (CH_3CH_2OH) for in-plane and out-of-plane directions were also investigated. In He*(2^3S) PIES,

[⊗] Abstract published in *Advance ACS Abstracts,* April 15, 1997.

S1089-5639(97)00156-4 CCC: $14.00

strong enhancement for ionization from MOs having sulfur 3s orbital (S_{3s}) character was observed, and synthesized EED spectra were compared with the observed PIES.

II. Experimental Section

The experimental apparatus for Penning ionization electron spectroscopy and He I ultraviolet photoelectron spectroscopy was reported previously.[17] Metastable atoms of He*(2^1S,2^3S) were produced by a discharge nozzle source with a tantalum hollow cathode, and the He*(2^1S) component was quenched by a water-cooled helium discharge lamp. He I ultraviolet photoelectron spectra (UPS) were measured by using the He I resonance photons (584 Å, 21.22 eV) produced by a discharge in pure helium gas. The kinetic energy of ejected electrons by Penning ionization or photoionization was measured by a hemispherical electrostatic deflection type analyzer using an electron collection angle 90° to the incident He*(2^3S) or photon beam. The background pressure in the reaction chamber was on the order of 10^{-7} Torr. We estimated the energy resolution of the electron energy analyzer to be 60 meV from the full width at half-maximum (fwhm) of the $Ar^+(^2P_{3/2})$ peak in the He I UPS. The transmission efficiency curve of the electron analyzer was determined by comparing our UPS data with those by Gardner and Samson[33] and Kimura et al.[34]

For collision-energy-resolved measurements, we have combined two techniques with the apparatus for efficient measurements; the two-dimensional measuring technique[21] and the cross-correlation time-of-flight (TOF) method.[22,35] The metastable beam of He*(2^3S) was pulsed by a mechanical pseudorandom chopper rotating at 400 Hz and then introduced into a reaction cell located at 504 mm downstream from the chopper disk. Kinetic energies and time-dependent counts of emitted electrons from sample molecules and a reference stainless steel plate inserted into the collision cell were stored in a 2 MB RAM. Electron energies were scanned by 35 meV step and a dwell time for the TOF measurement was 3 μs. The resolution of the analyzer was lowered to 250 meV. The time resolution of the cross-correlation TOF method determined both by the rotational frequency (400 Hz) and the number of slit elements (2×127) on the chopper disk was about 10 μs, which typically corresponds to ca. 20 meV of collision energy width at $E_c \sim$ 170 meV. The signals of secondary electrons emitted from the stainless steel plate were detected in electron energy range of 6−7 eV, which gives strong intensity of the secondary electrons. The observed two-dimensional spectra $I_e(E_e,t)$ as a function of electron kinetic energy E_e and time t were converted to time-dependent Penning ionization electron spectra $I_e(E_e,t_{TOF})$ by Hadamard transformation. The two-dimensional spectra $I_e(E_e,t_{TOF})$ can lead to $I_e(E_e,\nu_{He^*})$ as a function of the velocity of He* and then to the two-dimensional Penning ionization cross section $\sigma(E_e,\nu_r)$ by the equations

$$\sigma(E_e,\nu_r) = c\{I_e(E_e,\nu_{He^*})/I_{He^*}(\nu_{He^*})\}(\nu_{He^*}/\nu_r) \quad (3)$$

$$\nu_r = [\nu_{He^*}{}^2 + 3kT/M]^{1/2} \quad (4)$$

where c is a constant, ν_r is the relative velocity averaged over the velocity of the target molecule, k is the Boltzmann constant, and T and M are the gas temperature and the mass of the target molecule, respectively. Velocity distribution $I_{He^*}(\nu_{He^*})$ of He* beam was determined by monitoring secondary electrons emitted from the inserted stainless plate. Finally, $\sigma(E_e,\nu_r)$ is converted to $\sigma(E_e,E_c)$ as functions of E_e and collision energy (E_c) by the relation

$$E_c = \mu\nu_r{}^2/2 \quad (5)$$

where μ is the reduced mass of the system.

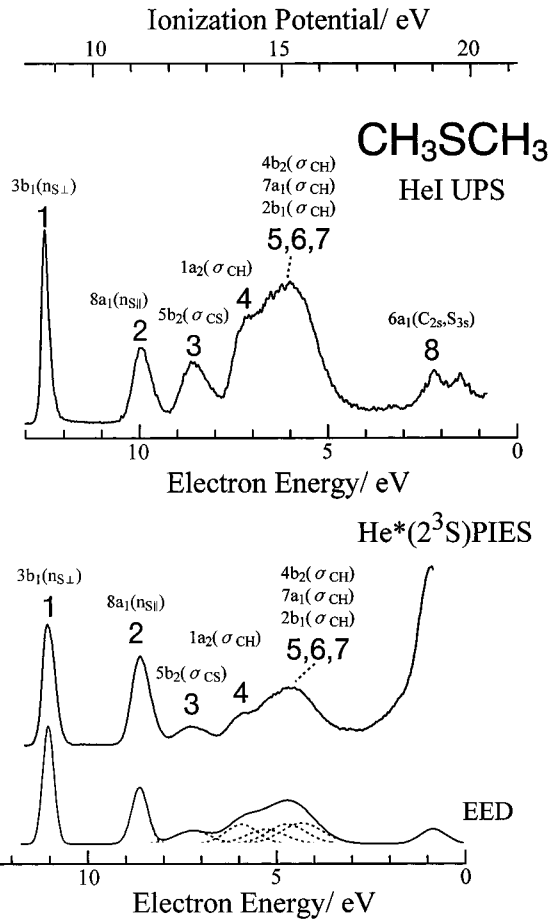

Figure 1. He I UPS, He*(2^3S) PIES, and synthesized EED spectrum of CH_3SCH_3. The electron energy resolution of UPS and PIES was 60 meV. For PIES, full He*(2^3S) beam was used (average collision energy is ~170 meV).

III. Calculations

We performed *ab initio* self-consistent field (SCF) calculations with 4-31G basis functions for neutral target molecules in order to obtain electron density contour maps, schematic diagrams of MOs, and orbital energies. The geometries of the molecules were selected from microwave spectroscopic studies for CH_3SCH_3,[36] CH_3SSCH_3,[37] CH_3CH_2SH,[38] and CH_3CH_2OH.[39] In electron density contour maps, thick solid curves indicate the repulsive molecular surface approximated by van der Waals radii.[40] In schematic diagrams of MOs, circles and ellipses were used as in previous studies.[8−10,19,20] Solid circles showed valence s orbitals, where couples of ellipses and dashed circles showed in-plane and out-of-plane component of p orbitals, respectively. In addition, we calculated EED values using SCF MOs obtained by 6-311+G basis functions which are known to give good agreement with experimental results of PIES[13] and electron momentum distribution.[41]

Interaction potential energies between He*(2^3S) and the target molecule for various directions were also calculated on the basis of the well-known resemblance between He*(2^3S) and Li(2^2S); the shape of the velocity dependence of total scattering cross section of He*(2^3S) by He, Ar, and Kr is very similar to that of Li,[42] and the location of the interaction potential well and its depth are very similar for He*(2^3S) and Li with various targets.[4,24,43] Because of these findings and difficulties associated with calculations for excited states, a lithium atom was used for model calculations of interaction potential energy instead of He*(2^3S). When we carried out model calculations for sulfur compounds with lithium atom using an unrestricted Hartree−Fock (UHF) method and second-order Møller−Plesset

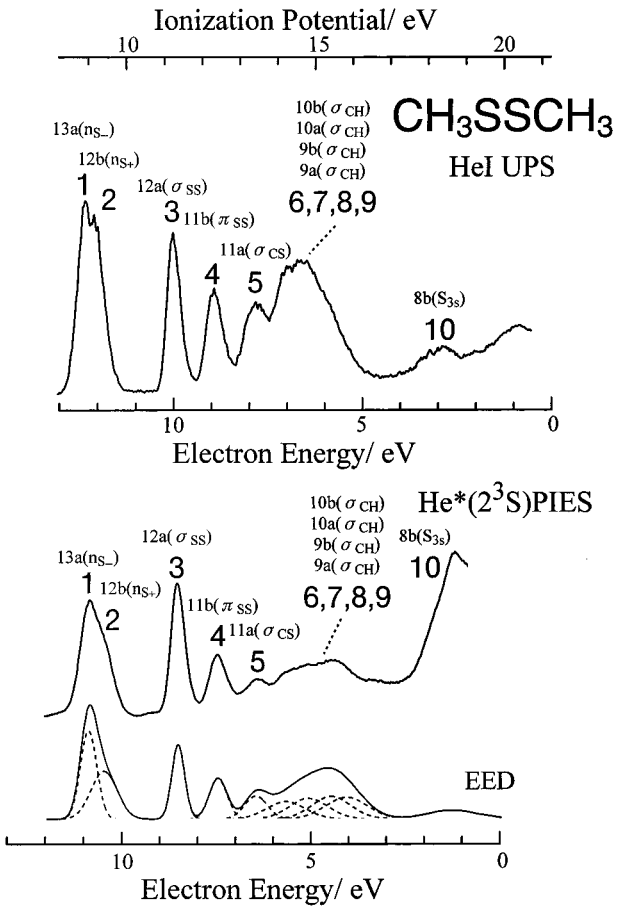

Figure 2. He I UPS, He*(2^3S) PIES, and synthesized EED spectrum of CH_3SSCH_3. The electron energy resolution of UPS and PIES was 60 meV. For PIES, full He*(2^3S) beam was used (average collision energy is ~170 meV).

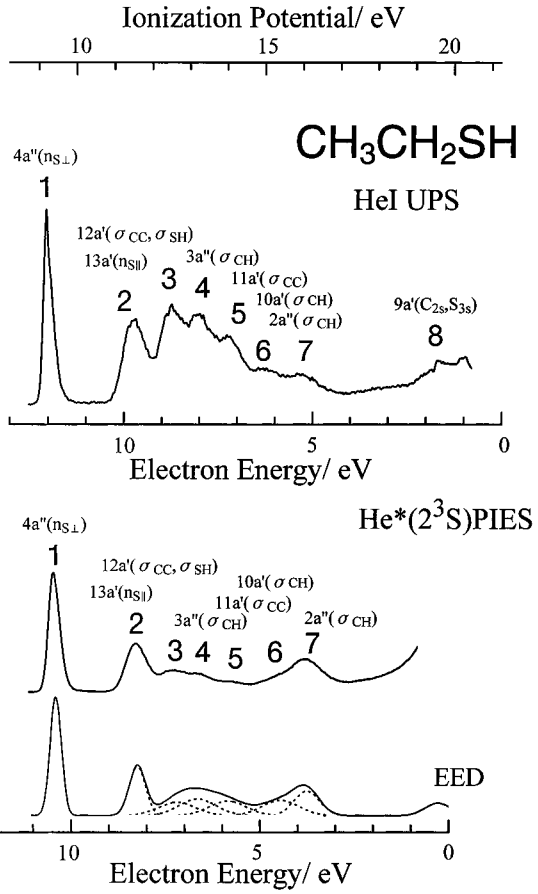

Figure 3. He I UPS, He*(2^3S) PIES, and synthesized EED spectrum of CH_3CH_2SH. The electron energy resolution of UPS and PIES was 60 meV. For PIES, full He*(2^3S) beam was used (average collision energy is ~170 meV).

(MP2) perturbation theory, the results were strongly spin-contaminated (*e.g.* the expected value of the spin angular momentum was 0.7541 for CH_3CH_2SH-Li complex (in-plane access to S atom, the distance is 2.0 Å)). Then we performed interaction potential calculations with a 4-31++G** basis set using a density functional theory (DFT), and the electron correlation was taken in Becke's three-parameter exchange with Lee, Young, and Parr correlation functional (B3LYP)[44] in order to avoid spin contamination problems. For comparison, the interaction energy values by MP2 calculations will also be mentioned in this paper.

All the *ab initio* and the DFT calculations in this study were carried out using a quantum chemistry program.[45]

IV. Results

Figures 1−4 show the He I UPS and He*(2^3S) PIES of CH_3SCH_3, CH_3SSCH_3, CH_3CH_2SH, and CH_3CH_2OH, respectively. The electron energy scales for PIES are shifted relative to those for the UPS by the difference in the excitation energies, 21.22 − 19.82 = 1.40 eV. Synthesized EED spectra, which were obtained from Gaussian-type functions with those intensities proportional to the respective EED values, are also shown in figures. Band positions and bandwidths were estimated from the observed PIES. For S_{3s} bands of CH_3SCH_3 and CH_3CH_2SH, band positions and bandwidths of S_{3s} bands were estimated from the observed UPS.

Figures 5−8 show the collision-energy-resolved PIES (CERPIES) of CH_3SCH_3, CH_3SSCH_3, CH_3CH_2SH, and CH_3CH_2OH, respectively. In order to gain enough intensities, CERPIES were obtained from the two-dimensional PIES within ca. 16 μs width of TOF. In each figure, the low-collision-energy (95−105 meV, average 100 meV) spectrum is shown by a solid curve, and the high-collision-energy (210−260 meV, average 230 meV) spectrum is shown by a dashed curve.

Figures 9−12 show the log σ vs log E_c plots of CEDPICS for CH_3SCH_3, CH_3SSCH_3, CH_3CH_2SH, and CH_3CH_2OH, respectively. The CEDPICS were obtained from the two-dimensional PIES within the full width at half-maximum (fwhm) of given bands in order to avoid the effect of noise around the bottom of each band. Some diffuse and overlapping bands are not distinguishable. The calculated electron density contour maps of the molecular orbitals are also shown in the figures with simplified diagrams indicating component atomic orbitals. For CH_3SCH_3, electron density contour maps for a_1 and b_2 orbitals are shown on the CSC plane, and those for the a_2 and b_1 orbitals are shown on a plane at the height of 1.85 Å (van der Waals radii of the sulfur atom) from the CSC plane. Similarly, electron density contour maps for a″ orbitals are shown on a plane at the height of 1.85 Å for CH_3CH_2SH or 1.40 Å (van der Waals radii of the oxygen atom) for CH_3CH_2OH from the CCX (X = S or O) plane, and those for the other orbitals are shown on the CCX plane. For CH_3SSCH_3, electron density contour maps are shown on the molecular plane which is vertical to the C_2 axis of symmetry and contains two carbon atoms (for 9a, 10a, 9b, and 10b orbitals) or two sulfur atoms (for the other orbitals).

Table 1 lists the vertical ionization potentials (IP determined from the He I UPS) and the assignments of the observed bands. The peak energy shifts (ΔE) in PIES measured with respect to the "nominal" energy E_0 (E_0 = the difference between the metastable excitation energy and the target ionization potential) are also shown. The peak energy shifts of some diffuse bands

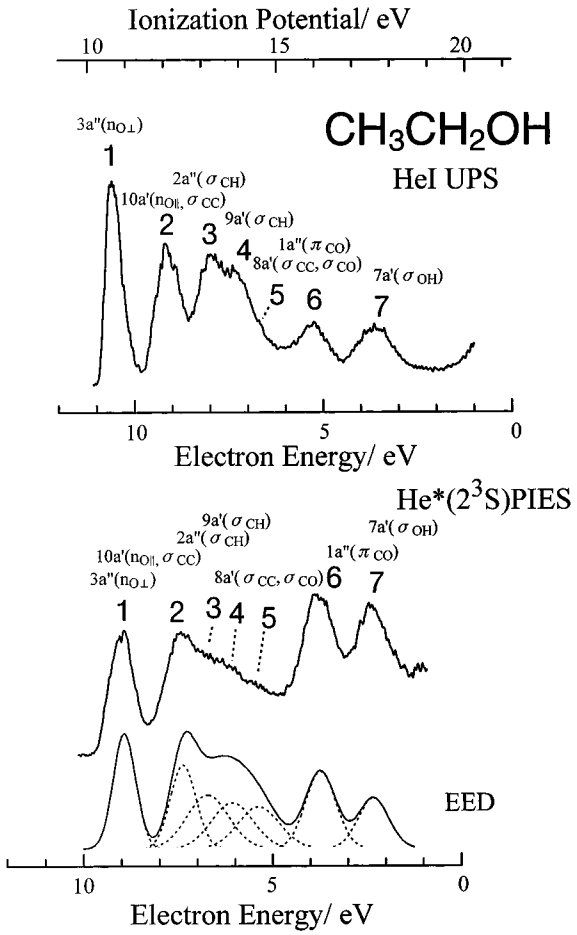

Figure 4. He I UPS, He*(2^3S) PIES, and synthesized EED spectrum of CH_3CH_2OH. The electron energy resolution of UPS and PIES was 60 meV. For PIES, full He*(2^3S) beam was used (average collision energy is ~170 meV).

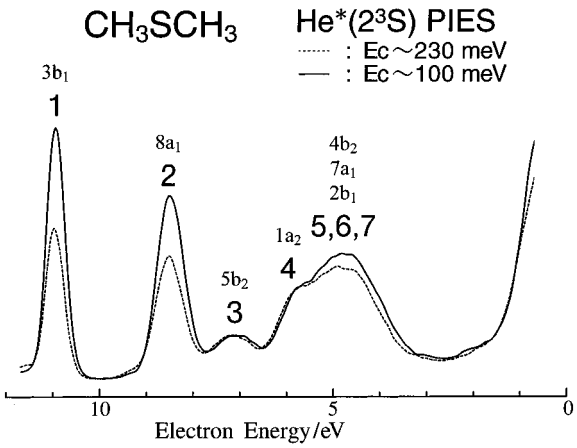

Figure 5. Collision-energy-resolved He*(2^3S) PIES of CH_3SCH_3 (solid curve at 95−105 meV, average 100 meV; dashed curve at 210−260 meV, average 230 meV) taken with an electron energy resolution of 250 meV.

or shoulders were not determined. Values of the slope parameter m for the log σ vs log E_c plots estimated in a collision energy range 95−260 meV by a linear least-squares method were also shown. The calculated EED values for corresponding MOs were also listed.

Figure 13 shows potential energy curves $V(R)$ as functions of the distance R between Li and CH_3SCH_3, CH_3CH_2SH, and CH_3CH_2OH for out-of-plane access vertical to the CSC or CCXH (X = S or O) plane and in-plane access. The lithium atom was placed on a bisector of CSC or CXH angle for in-plane access.

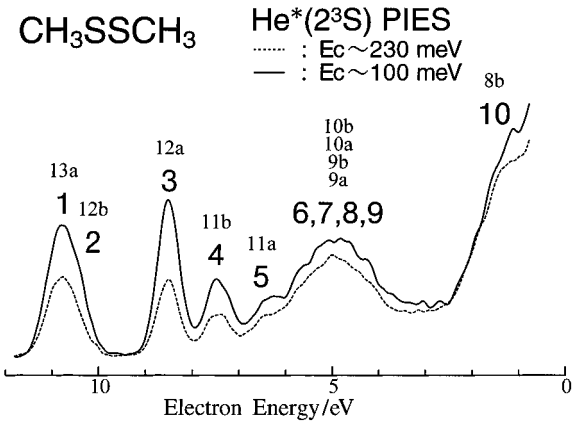

Figure 6. Collision-energy-resolved He*(2^3S) PIES of CH_3SSCH_3 (solid curve at 95−105 meV, average 100 meV; dashed curve at 210−260 meV, average 230 meV) taken with an electron energy resolution of 250 meV.

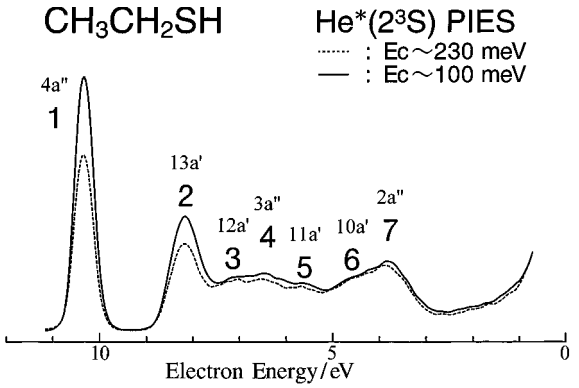

Figure 7. Collision-energy-resolved He*(2^3S) PIES of CH_3CH_2SH (solid curve at 95−105 meV, average 100 meV; dashed curve at 210−260 meV, average 230 meV) taken with an electron energy resolution of 250 meV.

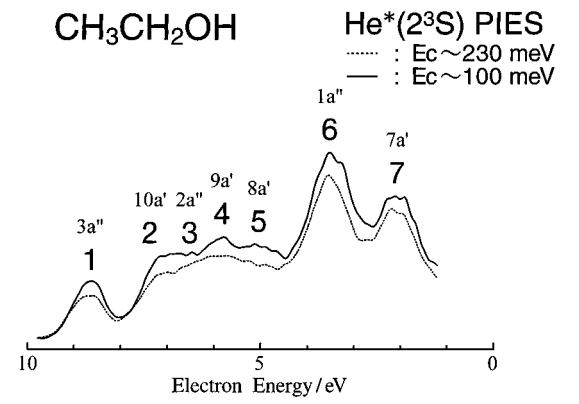

Figure 8. Collision-energy-resolved He*(2^3S) PIES of CH_3CH_2OH (solid curve at 95−105 meV, average 100 meV; dashed curve at 210−260 meV, average 230 meV) taken with an electron energy resolution of 250 meV.

Figure 14 shows potential energy curve $V(\theta)$ as a function of the angle θ between Li and CH_3SSCH_3 (θ is an angle from the axis vertical to the SSC plane). The angle of CS−Li ($\angle$CSLi = 154.5°) was determined by searching minimum energy around the S atom with the S−Li distance (R = 2.5 Å) fixed on the SSC plane.

V. Discussion

He I or He II UPS of CH_3SCH_3,[46−55] CH_3SSCH_3,[53−59] CH_3CH_2SH,[60] and CH_3CH_2OH[60−63] have been extensively investigated previously. The observed bands can be assigned to MOs according to the ordering of Koopmans' IP, and the IP values

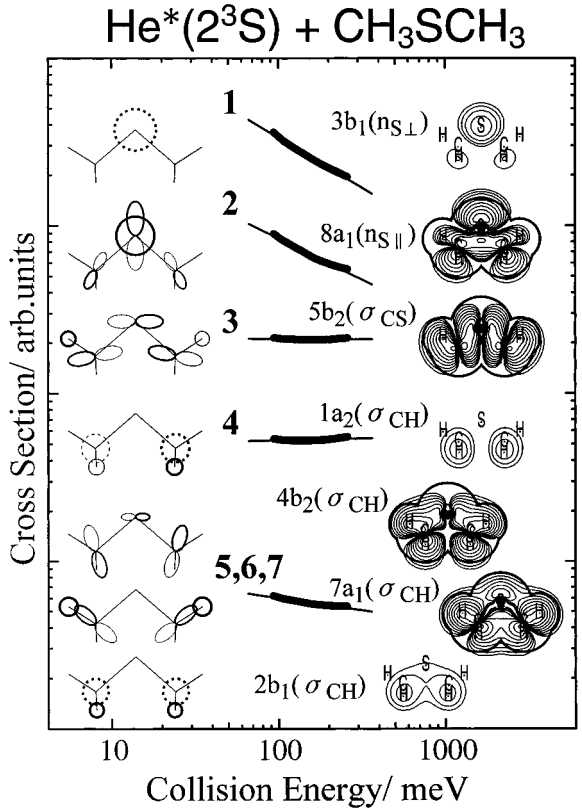

Figure 9. Collision energy dependence of partial ionization cross sections for CH_3SCH_3 with He*(2^3S). Electron density maps and schematic diagrams are shown for respective MOs.

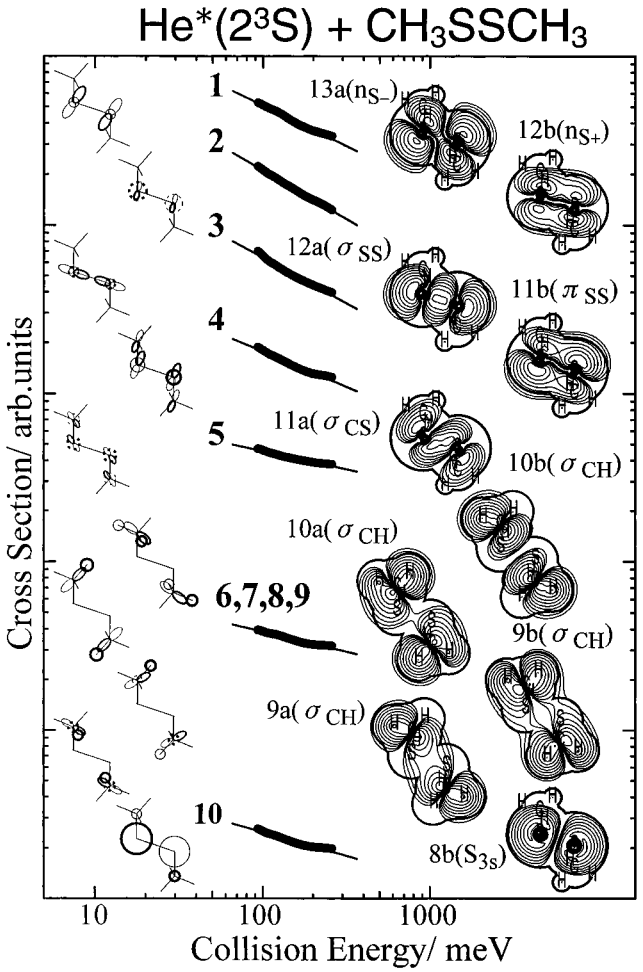

Figure 10. Collision energy dependence of partial ionization cross sections for CH_3SSCH_3 with He*(2^3S). Electron density maps and schematic diagrams are shown for respective MOs.

are listed in Table 1. Although He*(2^3S) PIES of CH_3CH_2SH[64] and CH_3CH_2OH[64,65] were measured, collision-energy-resolved measurements have not yet been made for these molecules.

A. CH_3SCH_3. In He*(2^3S) PIES (Figure 1), n_s bands originated from nonbonding sulfur orbitals and the S_{3s} band are strongly enhanced. The enhancement of n_s bands can be accounted for by the large EED value, whereas the intensity of S_{3s} band is in disagreement with the EED value. We will mention the reason of this discrepancy in section D.

By collision-energy-resolved Penning ionization electron spectroscopy (Figures 5 and 9), we observed strong negative collision energy dependence for band 1 ($m = -0.60$) and band 2 ($m = -0.49$) which originate from out-of-plane sulfur orbital ($n_{s\perp}$) and in-plane nonbonding sulfur orbital ($n_{s\parallel}$), respectively. These negative slopes indicate that the potential energy surface is attractive around the sulfur atom. When the long-range attractive part of the interaction potential $V^*(R)$ plays a dominant role and its form is the type

$$V^*(R) \propto R^{-s} \tag{6}$$

the collision energy dependence of $\sigma(E_c)$ can be expressed as

$$\log \sigma(E_c) \propto (-2/s) \log E_c \tag{7}$$

This equation gives a relationship between the slope parameter m and the potential parameter s ($m = -2/s$).[4,25,30] The s values obtained for ionization from nonbonding orbitals are listed in Table 1. Indeed, attractive potential wells have been found in the calculated curves (Figure 13) for the out-of-plane and in-plane direction access to the sulfur atom, and the trend of the steepness of the curves are consistent with the obtained s values (ca. 3.3 for the $n_{s\perp}$ band and ca. 4.1 for the $n_{s\parallel}$ band). In addition, negative peak shifts for the $n_{s\perp}$ band ($\Delta E = -130 \pm 10$ meV) and the $n_{s\parallel}$ band ($\Delta E = -50 \pm 30$ meV) indicate the existence of an attractive well of this order, and the estimated values are in good agreement with the calculated well depth of ca. 190 meV (ca. 210 meV by an MP2 calculation, $R = 2.6$ Å) for the out-of-plane direction and ca. 85 meV (ca. 100 meV by MP2 calculation, $R = 2.65$ Å) for the in-plane direction. The potential energy surface for CH_3SCH_3 was shown to be more attractive for the out-of-plane direction than for the in-plane direction, which is contrary to the case of CH_3OCH_3.[20] Small collision energy dependence had been observed for n_s band of CH_3NCS ($m = 0.014$)[18] and thiophene ($m = -0.15$).[10]

As discussed in the literature,[17] when the repulsive term is dominant in the reaction, the slope parameter m is related to the parameters d and b by the equation $m = (b/d) - 1/2$, where d is the effective decay parameter for the interaction potential between the target molecule and the metastale atom ($V^*(R) = B \exp(-dR)$; R is the distance) and b is the effective parameter of the transition probability ($W(R) = C \exp(-bR)$) related to the IP of the molecule (I(M)) by an equation $b = 2\{2I(\mathrm{M})\}^{1/2}$. A steep repulsive wall corresponding to a large d value can result in a (b/d) value smaller than 1/2 and a small dependence. Very small dependence of band 3 ($m = -0.01$) and band 4 ($m = 0.02$), which are related to the ionization from the $5b_2$ (σ_{CS}) and $1a_2$ (σ_{CH}) orbitals, can be ascribed to the electron density distribution in repulsive σ_{CH} bond region. Indeed, a repulsive potential energy curve was obtained for straight access to the σ_{CH} bond (Figure 13). In addition, small peak energy shifts of band 3 ($\Delta E = -60 \pm 100$ meV) and band 4 ($\Delta E = 70 \pm 130$ meV) can also be ascribed to the repulsive σ_{CH} bond region. For bands 5−7, all of the MOs ($4b_2$, $7a_1$, and $2b_1$) extend for

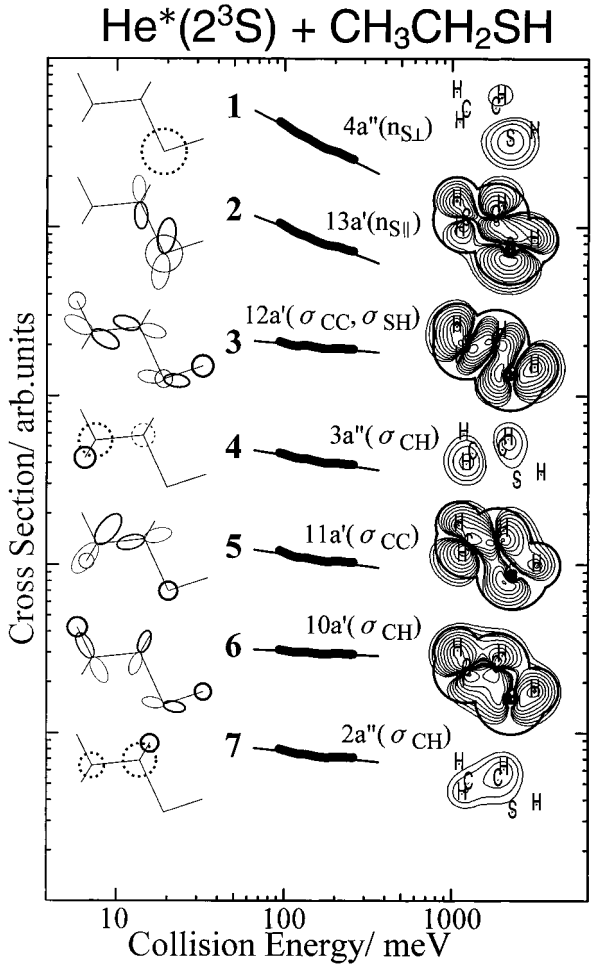

Figure 11. Collision energy dependence of partial ionization cross sections for CH_3CH_2SH with He*(2^3S). Electron density maps and schematic diagrams are shown for respective MOs.

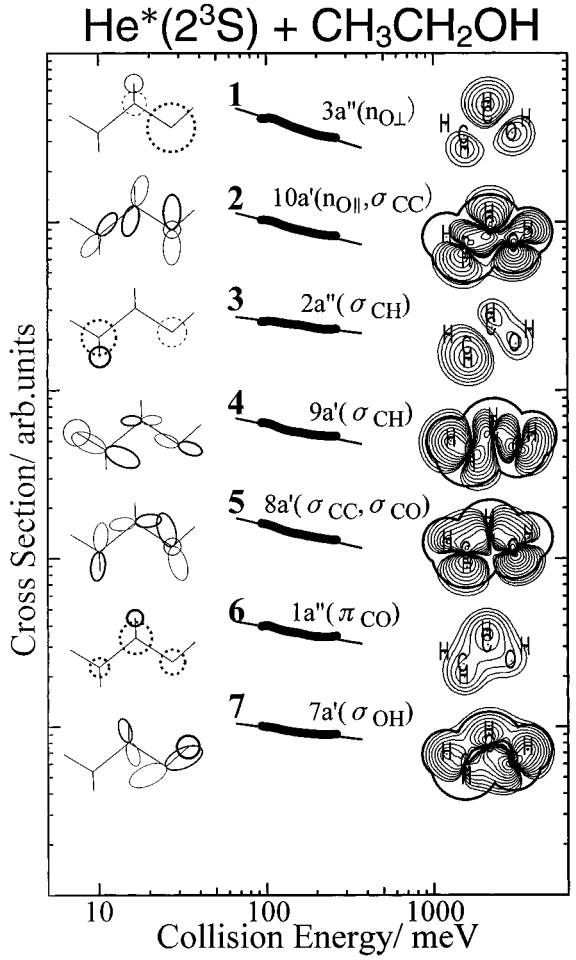

Figure 12. Collision energy dependence of partial ionization cross sections for CH_3CH_2OH with He*(2^3S). Electron density maps and schematic diagrams are shown for respective MOs.

the repulsive region around σ_{CH} bond and the attractive region around the sulfur atom for in-plane direction ($4b_2$ and $7a_1$) or out-of-plane direction ($2b_1$), which can result in the small negative slope of bands 5−7 ($m = -0.15$).

B. CH_3SSCH_3. The n_s bands (band 1 and band 2) and σ_{ss} band (band 3) in PIES are enhanced, which reflects the large values of EED as can be seen in Figure 2. The S_{3s} band is also enhanced. We will mention the reason of this enhancement later in section D.

The n_s bands originated from n_{s-} and n_{s+} orbitals which can be related with the $n_{s\perp}$ orbital of CH_3SCH_3 show strong negative collision energy dependence for band 1 ($m = -0.48$) and band 2 ($m = -0.57$) similar to the $n_{s\perp}$ band of CH_3SCH_3 ($m = -0.60$). Similarly, the σ_{SS} and π_{SS} bands which can be relatd with the $n_{s||}$ orbital of CH_3SCH_3 also show strong negative collision energy dependence for band 3 ($m = -0.54$) and band 4 ($m = -0.42$) similar to the $n_{s||}$ band of CH_3SCH_3 ($m = -0.49$). For these two sets of related bands, negative dependence of band 1 (n_{s-}, $m = -0.48$) and band 4 (π_{SS}, $m = -0.42$) is weaker than band 2 (n_{s+}, $m = -0.57$) and band 3 (σ_{SS}, $m = -0.54$), respectively. As can be seen in Figure 14, the calculated interaction potential energy curve deformed upward near $\theta = 0°$ shows the effect of repulsive potential around the methyl group for out-of-plane direction. Comparing the deformed potential energy curve with the most effective collisional directions suggested by the electron distribution of each MOs exposed outside the molecular surface (direction 1−4), the weaker dependence for band 1 than band 2 as well as band 4 than band 3 can be explained by the effect of repulsive potential around the methyl group for the out-of-plane 1 and 4 directions rather than for 2 and 3 directions. In addition, the negative peak energy shifts about −100 meV for bands 1 ($\Delta E = -95 \pm 30$ meV), band 3 ($\Delta E = -110 \pm 30$ meV), and band 4 ($\Delta E = -85 \pm 30$ meV) are in good agreement with the calculated potential energy, while band 2 is on the shoulder of band 1 and it is difficult to estimate precise negative peak energy shift.

Small negative collision energy dependence for σ_{CS} band (band 5, $m = -0.22$) and σ_{CH} bands (bands 6−9, $m = -0.24$) can be ascribed to the repulsive potential energy surface around the σ_{CH} orbital region and attractive interaction potential around the sulfur atoms for the twisted out-of-plane direction by the dihedral angle of CSS/SSC planes (84.52°).[36]

To sum up, the trend of similar collision energy dependence for the in-plane and the out-of-plane directions of CH_3SCH_3 is also found for CH_3SSCH_3, especially around the sulfur atoms.

C. CH_3CH_2SH and CH_3CH_2OH. In He*(2^3S) PIES, the $n_{s\perp}$ band of CH_3CH_2SH is enhanced and sharp in comparison with the $n_{s||}$ band (Figure 3), while the $n_{O\perp}$ band of CH_3CH_2-OH is comparable with $n_{O||},\sigma_{CC}$ band (Figure 4). Contrary to the delocalized $n_{O\perp}$ orbital with EED value of 3.32, the $n_{s\perp}$ orbital has nearly pure nonbonding 3p nature and a large EED value (7.03). Similarly, the EED value of the $n_{s||}$ orbital is large (4.17) in spite of a relatively large 3s component, while the EED value of the delocalized $n_{O||},\sigma_{CC}$ orbital is small (2.76).

For CH_3CH_2SH, strong negative collision energy dependence for band 1 ($m = -0.51$) and band 2 ($m = -0.38$) was observed in CERPIES (Figure 7) and CEDPICS (Figure 11). By model calculation, it was confirmed that the potential energy surface for the out-of-plane access to the sulfur atom of CH_3CH_2SH is more attractive than the in-plane access (Figure 13), and the

TABLE 1: Band Assignments, Ionization Potential (IP), Peak Energy Shift (ΔE), Obtained Parameter Values (m, s), and EED Values (See Text)

molecule	band	IP_{obsd}	IP_{calcd}	orbital	ΔE/meV	m	s	EED value
CH_3SCH_3								
	1	8.72	9.16	$3b_1(n_{s\perp})$	-130 ± 10	-0.60	3.3	6.15
	2	11.27	11.56	$8a_1(n_{s\|\|})$	-50 ± 30	-0.49	4.1	4.20
	3	12.57	13.21	$5b_2(\sigma_{CS})$	-60 ± 100	-0.01		2.14
	4	14.12	15.42	$1a_2(\sigma_{CH})$	70 ± 130	0.02		2.87
	5	(15.0)	15.81	$4b_2(\sigma_{CH})$				2.54
	6	(15.3)	16.52	$7a_1(\sigma_{CH})$		-0.15		3.47
	7	(15.6)	16.55	$2b_1(\sigma_{CH})$				3.95
	8	19.02	21.98	$6a_1(C_{2s},S_{3s})$				1.76
CH_3SSCH_3								
	1	8.94	9.61	$13a(n_{s-})$	-95 ± 30	-0.48	4.2	5.74
	2	9.16	9.90	$12b(n_{s+})$		-0.57	3.5	4.98
	3	11.23	11.74	$12a(\sigma_{SS})$	-110 ± 30	-0.54	3.7	3.85
	4	12.32	13.32	$11b(\pi_{SS})$	-85 ± 30	-0.42	4.8	2.90
	5	13.41	14.43	$11a(\sigma_{CS})$	-30 ± 150	-0.22		2.08
	6	14.24	15.91	$10b(\sigma_{CH})$	-180 ± 200			2.69
	7	(14.6)	16.38	$10a(\sigma_{CH})$				3.19
	8	(14.8)	16.47	$9b(\sigma_{CH})$		-0.24		3.51
	9	(15.2)	16.78	$9a(\sigma_{CH})$				3.66
	10	18.42	21.53	$8b(S_{3s})$	-200 ± 100	-0.28		1.65
CH_3CH_2SH								
	1	9.29	9.68	$4a''(n_{s\perp})$	-130 ± 30	-0.51	3.9	7.03
	2	11.57	11.97	$13a'(n_{s\|\|})$	0 ± 50	-0.38	5.3	4.17
	3	12.59	13.42	$12a'(\sigma_{CC},\sigma_{SH})$	-30 ± 150	-0.09		2.58
	4	13.27	13.95	$3a''(\sigma_{CH})$	70 ± 100	-0.16		3.24
	5	14.06	14.68	$11a'(\sigma_{CC})$	15 ± 120	-0.14		2.83
	6	15.02	16.79	$10a'(\sigma_{CH})$		-0.05		2.98
	7	15.91	17.28	$2a''(\sigma_{CH})$	-160 ± 150	-0.11		3.31
	8	19.65	22.35	$9a'(C_{2s},S_{3s})$				1.69
CH_3CH_2OH								
	1	10.63	11.88	$3a''(n_{O\perp})$	-350 ± 50	-0.31	6.5	3.32
	2	12.04	13.16	$10a'(n_{O\|\|},\sigma_{CC})$	-450 ± 100	-0.25	8.0	2.76
	3	13.23	14.26	$2a''(\sigma_{CH})$	-50 ± 200	-0.13		2.87
	4	13.82	14.34	$9a'(\sigma_{CH})$	-100 ± 200	-0.20		2.46
	5	(14.5)	15.33	$8a'(\sigma_{CC},\sigma_{CO})$		-0.24		2.24
	6	15.90	17.63	$1a''(\pi_{CO})$	-210 ± 100	-0.18		3.02
	7	17.57	18.72	$7a'(\sigma_{OH})$	100 ± 50	-0.13		1.98

trend of the steepness of the curves is consistent with the s values of ca. 3.9 and ca. 5.3 obtained by m values for the $n_{s\perp}$ band and the $n_{s||}$ band, respectively. Negative peak shifts for the $n_{s\perp}$ band ($\Delta E = -130 \pm 30$ meV) and the $n_{s||}$ band ($\Delta E = 0 \pm 50$ meV) are in good agreement with the calculated well depth of ca. 190 meV (ca. 190 meV by an MP2 calculation, $R = 2.6$ Å) for the out-of-plane direction and ca. 50 meV (ca. 40 meV by an MP2 calculation, $R = 2.85$ Å) for the in-plane direction. The similar trend of anisotropic potential energy surface was observed for CH_3SCH_3. On the other hand, the σ_{CH} bands (bands 3−7) show weak negative dependence ($m = -0.09 \sim -0.16$), which is thought to be due to the repulsive σ_{CH} orbital region.

For CH_3CH_2OH, the negative peak energy shifts were observed for the $n_{O\perp}$ band ($\Delta E = -350 \pm 50$ meV) and the $n_{O||},\sigma_{CC}$ band ($\Delta E = -450 \pm 100$ meV). The calculated well depth (Figure 13) of out-of-plane direction (ca. 200 meV) and in-plane direction (ca. 400 meV) agrees with the estimated values from the peak energy shift. Contrary to those for CH_3SCH_3 and CH_3CH_2SH, the potential energy surfaces for in-plane access to the oxygen atom of CH_3OCH_3[20] and CH_3CH_2OH were calculated to be more attractive than the out-of-plane access. In the long range, the steepness of the calculated curves for the out-of-plane access and the in-plane access is, however, not consistent with the s values of ca. 6.5 and ca. 8.0 obtained by m values for band 1 ($n_{O\perp}$, $m = -0.31$) and band 2 ($n_{O||},\sigma_{CC}$, $m = -0.25$), respectively. This discrepancy can be ascribed to the σ_{CC} character of the 10a′ orbital for band 2. Relatively small slopes of band 3 ($m = -0.13$), band 6 ($m = -0.18$), and band 7 ($m = -0.13$) can be ascribed to the MOs extending to the out-of-plane direction (2a″ and 1a″) or σ_{CH} bond region (7a′). On the other hand, negative collision energy dependence of band 4 ($m = -0.20$) and band 5 ($m = -0.24$) can be ascribed to the MOs extending around the oxygen atom for the in-plane direction (9a′ and 8a′). Different from CH_3CH_2SH, intensities of band 6 and band 7 are relatively large, which is thought to be due to small intensities of band 1 and band 2 as can be seen in the EED values. Relative intensities in a background-subtracted PIES normalized by band 1 (100 ± 10) were estimated[65] to be 128 ± 25 for band 6 and 100 ± 20 for band 7, respectively.

The $|m|$ values for n_s bands of CH_3CH_2SH were relatively large in comparison with n_O bands of CH_3CH_2OH, which is also true for CH_3SCH_3 and CH_3OCH_3.[20] The steepness of long-range attractive part of the interaction potential curves (Figure 13) is consistent with the observed m values, while the position of repulsive wall in the calculated potential curves reflects simply the size of the sulfur or oxygen atom. From the small s values of n_s bands, the long-range attractive interaction can be connected with charge-induced force ($s = 4$). Recently, He I UPS for charge-transfer complexes of bromine with EtSEt and EtOEt have been studied,[66] and the geometries of these $n-\sigma^*$ complexes were computed to be a C_s form for $(Et)_2S\cdots Br_2$ with higher binding energy than the $(Et)_2O\cdots Br_2$ complex (C_{2v} form), which shows anisotropic interaction of $(Et)_2S$ out-of-plane dirction and $(Et)_2O$ for the in-plane direction. The anisotropic potential energy surface and s values of the sulfur compounds with He* metastable atom, therefore, are thought to be explained by charge-transfer and the charge-induced attractive long-range force for the out-of-plane direction.

D. Enhanced Sulfur 3s Bands. The enhanced intensities for the sulfur 3s (S_{3s}) bands observed in He*(2^3S) PIES are not consistent with the synthesized EED spectra, while other band intensities agree with the EED spectra (Figures 1−3). In the

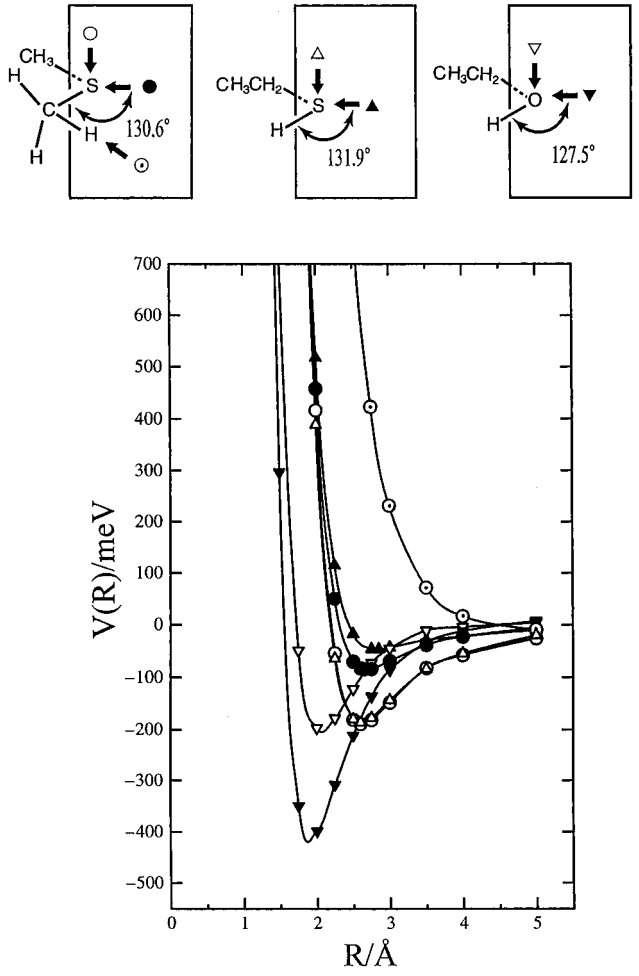

Figure 13. Interaction potential curves $V(R)$ for CH_3SCH_3-Li, CH_3CH_2SH-Li, and CH_3CH_2OH-Li: (○) out-of-plane access to the S atom of CH_3SCH_3; (●) in-plane access to the S atom of CH_3SCH_3; (⊙) straight access to the methyl group of CH_3SCH_3; (△) out-of-plane access to the S atom of CH_3CH_2SH; (▲) in-plane access to the S atom of CH_3CH_2SH; (▽) out-of-plane access to the O atom of CH_3CH_2OH; (▼) in-plane access to the O atom of CH_3CH_2OH. R is the distance between the Li atom and S, O, or C atoms.

case of previous study[12] of $(CH_3)_4C$ and $(CH_3)_3CCl$, enhancement of inner valence carbon 2s (C_{2s}) bands in PIES was found to be caused by an intermolecular excitation transfer ($He^*(2^3S) + M \rightarrow He + M^*$) involving C_{2s} hole in the target molecule followed by intramolecular Auger-like autoionization process ($M^* \rightarrow M^+ + e^-$) involving electronic transition from an upper occupied MO having C_{2s} character to the inner C_{2s} hole. Key factors for the highly selective Auger-like ionization are (a) orbital energies of A* and M for the resonant excitation transfer and (b) overlap between the MOs which have a relation to the intramolecular electronic transition. This Auger-like ionization mechanism can be suggested from the observed characters of extremely enhanced relative band intensity of PIES relative to the EED spectrum, which cannot be explained by the exchange ionization process of outer valence MOs, and from small collision energy dependence.[12] For CH_3SSCH_3, an ESCA spectrum[67] has shown that the binding energy for a bonding S_{3s} orbital ($\sigma(S_{3s}+S_{3a})$,7a) is larger than that of antibonding S_{3s} orbital ($\sigma(S_{3s}-S_{3s})$,8b) by 6.7 eV, which gives the orbital energy of 25.1 eV (= 18.4 + 6.7) near to the approximate 1s orbital energy (24.59 eV) of $He^*(2^3S)$ obtained from ionization energy of He atom. In addition, the 2s orbital energy of $He^*(2^3S)$ is estimated to be −4.77 eV (= −24.59 + 19.82), which is comparable with the energy of an unoccupied MO (−3.98 eV) estimated from the first ionization energy (8.94 eV) and a transition energy (4.96 eV).[68] Furthermore, the S_{3s} band of CH_3SSCH_3 shows smaller collision energy dependence ($m = -0.28$) than bands 1−4 ($m = -0.42 \sim -0.57$) originated from the MOs whose electron densities localized on the sulfur atoms. By these findings, resonant excitation transfer and the following autoionization can be expected for S_{3s} band of CH_3SSCH_3 as observed C_{2s} bands of $(CH_3)_4C$ and $(CH_3)_3CCl$.[12]

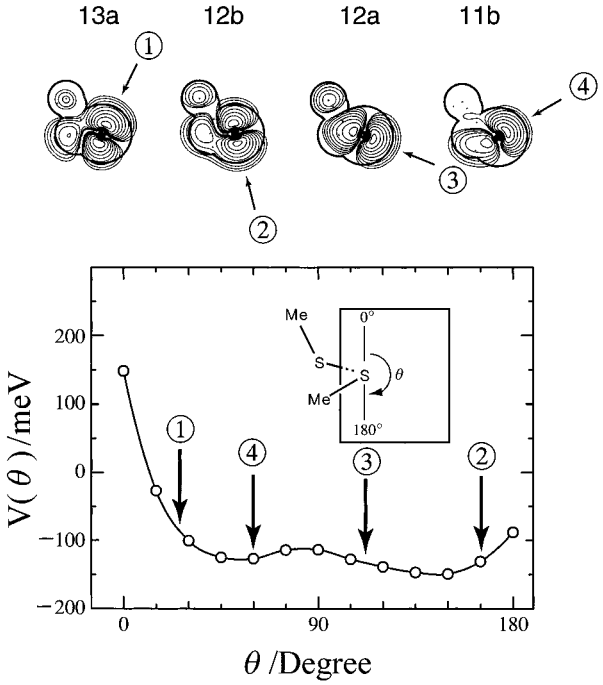

Figure 14. Interaction potential curve $V(\theta)$ for CH_3SSCH_3-Li (R = 2.5 Å) and electron density contour maps of 13a, 12b, 12a, and 11b orbitals of CH_3SSCH_3. Most effective directions are indicated by arrows.

Judging from the weak collision energy dependence observed in CERPIES (Figures 5 and 7), the enhancement in $He^*(2^3S)$ PIES at electron energy of ca. 1 eV or less for CH_3SCH_3 and CH_3CH_2SH can also be ascribed to the Auger-like ionization process as observed for CH_3SSCH_3. In He I UPS of CH_3SCH_3 and CH_3CH_2SH, S_{3s} bands were observed to be split. The reason of this splitting is unknown.

In the PIES of CH_3SSCH_3, a weak band at electron energy of ca. 3−3.5 eV was observed. In previous studies, the intensity of an electron correlation band showed similar collision energy dependence to another band which was related to an excitation upon the ionization.[7−10] This weak band of CH_3SSCH_3 can be ascribed to a satellite of the S_{3s} band because of the similar slope of CEDPICS ($m = -0.31$) with the S_{3s} band ($m = -0.28$).

VI. Conclusions

Collision energy dependence of the partial ionization cross sections has reflected the anisotropic potential energy surface of CH_3SCH_3, CH_3SSCH_3, and CH_3CH_2SH with $He^*(2^3S)$ atoms. The characteristic trends in the anisotropy are in common with these aliphatic sulfur compounds; interaction potentials around the sulfur atom are more attractive for the out-of-plane direction than for the in-plane direction, and the potential is repulsive around the alkyl group. The trend of the anisotropic attractive interaction around the sulfur atom was in good contrast to that around the oxygen atom of aliphatic oxygen compounds.

In $He^*(2^3S)$ PIES, n_S bands and S_{3s} bands were enhanced, while n_O bands were not so enhanced. The large intensity of n_S bands and the small intensity of n_O bands are consistent with the simulated branching ratios by exterior electron density (EED) model based on the electron-exchange ionization process. The enhancement of S_{3s} bands and weak negative collision energy dependence indicate that an intramolecular excitation transfer

between He* and M involving an S_{3s} type hole ($He^*(2^3S) + M \rightarrow He + M^*$) followed by an intramolecular autoionization process ($M^* \rightarrow M^+ + e^-$) is induced as proposed for C_{2s} bands of $(CH_3)_4C$ and $(CH_3)_3CCl$ by Takami et al.[12]

Acknowledgment. This work has been supported by a Grant in Aid for Scientific Research from the Japanese Ministry of Education, Science, and Culture.

References and Notes

(1) Penning, F. M. *Naturwissenshaften* **1927**, *15*, 818.
(2) Ḥotop, H.; Niehaus, A. *Z. Phys.* **1969**, *228*, 68.
(3) Čermák, V. *J. Chem. Phys.* **1966**, *44*, 3781.
(4) Niehaus, A. *Adv. Chem. Phys.* **1981**, *45*, 399.
(5) Yencha, A. J. *Electron Spectroscopy: Theory, Technique, and Application*; Brundle, C. R.; Baker, A. D., Eds.; Academic: New York, 1984; Vol. 5.
(6) Ohno, K.; Mutoh, H.; Harada, Y. *J. Am. Chem. Soc.* **1983**, *105*, 4555.
(7) Takami, T.; Ohno, K. *J. Chem. Phys.* **1992**, *96*, 6523.
(8) Ohno, K.; Kishimoto, N.; Yamakado, H. *J. Phys. Chem.* **1995**, *99*, 9687.
(9) Ohno, K.; Okamura, K.; Yamakado, H.; Hoshino, S.; Takami, T.; Yamauchi, M. *J. Phys. Chem.* **1995**, *99*, 14247.
(10) Kishimoto, N.; Yamakado, H.; Ohno, K. *J. Phys. Chem.* **1996**, *100*, 8204.
(11) Mitsuke, K.; Takami, T.; Ohno, K. *J. Chem. Phys.* **1989**, *91*, 1618.
(12) Takami, T.; Mitsuke, K.; Ohno, K. *J. Chem. Phys.* **1991**, *95*, 918.
(13) Ohno, K.; Harada, Y. In *Theoretical Models of Chemical Bonding*; Maksić, Z. B., Ed.; Springer-Verlag: Berlin-Heidelberg, 1991; Part 3, p 199 and reference cited therein.
(14) Ohno, K.; Ishida, T. *Int. J. Quantum Chem.* **1986**, *29*, 677.
(15) Dunlavy, D. C.; Martin, D. W.; Siska, P. E. *J. Chem. Phys.* **1990**, *93*, 5347.
(16) Longley, E. J.; Dunlavy, D. C.; Falcetta, M. F.; Bevsek, H. M.; Siska, P. E. *J. Phys. Chem.* **1993**, *97*, 2097.
(17) Ohno, K.; Takami, T.; Mitsuke, K.; Ishida, T. *J. Chem. Phys.* **1991**, *94*, 2675.
(18) Pasinszki, T.; Yamakado, H.; Ohno, K. *J. Phys. Chem.* **1993**, *97*, 12718.
(19) Pasinszki, T.; Yamakado, H.; Ohno, K. *J. Phys. Chem.* **1995**, *99*, 14678.
(20) Yamakado, H.; Yamauchi, M.; Hoshino, S.; Ohno, K. *J. Phys. Chem.* **1995**, *99*, 17093.
(21) Ohno, K.; Yamakado, H.; Ogawa, T.; Yamata, T. *J. Chem. Phys.* **1996**, *105*, 7536.
(22) Kishimoto, N.; Aizawa, J.; Yamakado, H.; Ohno, K. Submitted for publication.
(23) Yamauchi, M.; Yamakado, H.; Ohno, K. Submitted for publication.
(24) Hotop, H. *Radiat. Res.* **1974**, *59*, 379.
(25) Illenberger, E.; Niehaus, A. *Z. Phys. B* **1975**, *20*, 33.
(26) Parr, T. P.; Parr, D. M.; Martin, R. M. *J. Chem. Phys.* **1982**, *76*, 316.
(27) Pesnelle, A.; Watel, G.; Manus, C. *J. Chem. Phys.* **1975**, *62*, 3590.
(28) Woodard, M. R.; Sharp, R. C.; Seely, M.; Muschlitz, E. E., Jr. *J. Chem. Phys.* **1978**, *69*, 2978.
(29) Appoloni, L.; Brunetti, B.; Hermanussen, J.; Vecchiocattivi, F.; Volpi, G. G. *J. Chem. Phys.* **1987**, *87*, 3804.
(30) Allison, W.; Muschlitz, E. E., Jr. *J. Electron Spectrosc. Relat. Phenom.* **1981**, *23*, 339.
(31) Riola, J. P.; Howard, J. S.; Rundel, R. D.; Stebbings, R. F. *J. Phys. B* **1974**, *7*, 376.
(32) Lindinger, W.; Schmeltekopf, A. L.; Fehsenfeld, F. C. *J. Chem. Phys.* **1974**, *61*, 2890.
(33) Gardner, J. L.; Samson, J. A. R. *J. Electron Spectrosc. Relat. Phenom.* **1976**, *8*, 469.
(34) Kimura, K.; Katsumata, S.; Achiba, Y.; Yamazaki, T.; Iwata, S. *Handbook of He I Photoelectron Spectra of Fundamental Organic Molecules*; Japan Scientific: Tokyo, 1981.
(35) Auerbach, D. J. *Atomic and Molecular Beam Methods*; Scoles, G., Ed.; Oxford University: New York, 1988; p 369.
(36) Pierce, L.; Hayashi, M. *J. Chem. Phys.* **1961**, *35*, 479.
(37) Meyer, M. *J. Mol. Struct.* **1992**, *273*, 99.
(38) Hayashi, M.; Imaishi, H.; Kuwada, K. *Bull. Chem. Soc. Jpn.* **1974**, *47*, 2382.
(39) Callomon, J. H.; Hirota, E.; Kuchitsu, K.; Lafferty, W. J.; Maki, A. G.; Pote, C. S. *Landolt-Bornstein New Series Supplement II/7*; Springer: Berlin, 1976.
(40) Pauling, L. *The Nature of the Chemical Bond*; Cornell University: Ithaca, New York, 1960.
(41) Bawagan, A. O.; Müller-Fiedler, R.; Brion, C. E.; Davidson, E. R.; Boyle, C. *Chem. Phys.* **1988**, *120*, 335.
(42) Rothe, E. W.; Neynaber, R. H.; Trujillo, S. M. *J. Chem. Phys.* **1965**, *42*, 3310.
(43) Haberland, H.; Lee, Y. T.; Siska, P. E. *Adv. Chem. Phys.* **1981**, *45*, 487.
(44) Becke, A. D. *J. Chem. Phys.* **1993**, *7*, 5648.
(45) Frisch, C. M. J.; Trucks, G. W.; Head-Gordon, M.; Gill, P. M.; Wong, M. W.; Foresman, J. B.; Johnson, B. G.; Schlegel, H. B.; Robb, M. A.; Replogle, E. S.; Gomperts, R.; Andres, J. L.; Raghavachari, K.; Binkley, J. S.; Gonzalez, C.; Martin, R. L.; Fox, D. J.; Defrees, D. J.; Baker, J.; Stewart, J. J. P.; Pople, J. A. *Gaussian 92/DFT*; Gaussian, Inc.: Pittsburgh, PA, 1992.
(46) Cullen, W. R.; Frost, D. C.; Vroom, D. A. *Inorg. Chem.* **1969**, *8*, 1803.
(47) Cradock, S.; Whiteford, R. A. *J. Chem. Soc., Faraday Trans. 2* **1972**, *68*, 281.
(48) Frost, D. C.; Herring, F. G.; Katrib, A.; McDowell, C. A.; McLean, R. A. N. *J. Phys. Chem.* **1972**, *76*, 1030.
(49) Mollère, P.; Bock, H.; Becker, G.; Fritz, G. *J. Organomet. Chem.* **1973**, *61*, 127.
(50) Bünzli, J. C.; Frost, D. C.; Weiler, L. *J. Am. Chem. Soc.* **1973**, *95*, 7880.
(51) Schweig, A.; Thiel, W. *Mol. Phys.* **1974**, *27*, 265.
(52) Aue, D. A.; Webb, H. M.; Davidson, W. R.; Vidal, M.; Bowers, M. T.; Goldwhite, H.; Vertal, L. E.; Douglas, J. E.; Kollman, P. A.; Kenyon, G. L. *J. Am. Chem. Soc.* **1980**, *102*, 5151.
(53) Wagner, G.; Bock, H. *Chem. Ber.* **1974**, *107*, 68.
(54) Kobayashi, T. *Phys. Lett. A* **1978**, *69*, 31.
(55) Chang, F. C.; Young, V. Y.; Prater, J. W.; Cheng, K. L. *J. Electron Spectrosc. Relat. Phenom.* **1986**, *40*, 363.
(56) Baker, A. D.; Brisk, M.; Gellender, M. *J. Electron Spectrosc. Relat. Phenom.* **1974**, *3*, 227.
(57) Colton, R. J.; Rabalais, J. W. *J. Electron Spectrosc. Relat. Phenom.* **1974**, *3*, 345.
(58) Guimon, M. F.; Guimon, C.; Pfister-Guillouzo, G. *Tetrahedron Lett.* **1975**, *7*, 441.
(59) Kimura, K.; Osafune, K. *Bull. Chem. Soc. Jpn.* **1975**, *48*, 2421.
(60) Ogata, H.; Onizuka, H.; Nihei, Y.; Kamada, H. *Bull. Chem. Soc. Jpn.* **1973**, *46*, 3036.
(61) Katsumata, S.; Iwai, T.; Kimura, K. *Bull. Chem. Soc. Jpn.* **1973**, *46*, 3391.
(62) Baker, A. D.; Betteridge, D.; Kemp, N. R.; Kirby, R. E. *Anal. Chem.* **1971**, *43*, 375.
(63) Potts, A. W.; Williams, T. A.; Price, W. C. *Faraday Discuss. Chem. Soc.* **1972**, *54*, 104.
(64) (a) Ohno, K.; Imai, K.; Matsumoto, S.; Harada, Y. *J. Phys. Chem.* **1983**, *87*, 4346. (b) Ohno, K.; Imai, K.; Harada, Y. *J. Am. Chem. Soc.* **1985**, *107*, 8078.
(65) Yee, D. S. C.; Hamnett, A.; Brion, C. E. *J. Electron Spectrosc. Relat. Phenom.* **1976**, *8*, 291.
(66) Ananthavel, S. P.; Salai Cheettu Ammal, S.; Venuvanalingam, P.; Chandrasekhar, J.; Hegde, M. S. *Chem. Phys. Lett.* **1994**, *228*, 431.
(67) Riga, J.; Verbist, J. J.; Lamotte, C.; Andre, J. M. *Bull. Soc. Chim. Belg.* **1978**, *87*, 163.
(68) Thompson, S. D.; Carroll, D. G.; Watson, F.; O'Donnell, M.; McGlynn, S. P. *J. Chem. Phys.* **1966**, *45*, 1367.